Characterization of Surface-Wave and Leaky-Wave Propagation on Wire-Medium Slabs and Mushroom Structures Based on Local and Nonlocal Homogenization Models

Alexander B. Yakovlev, *Senior Member, IEEE*, Mário G. Silveirinha, *Member, IEEE*, Olli Luukkonen, Constantin R. Simovski, *Member, IEEE*, Igor S. Nefedov, *Member, IEEE*, and Sergei A. Tretyakov, *Fellow, IEEE*

***Abstract*—In this paper, a nonlocal homogenization model is proposed for the analysis of the spectrum of natural modes on sub-wavelength mushroom-type high-impedance surfaces composed of a capacitive grid connected to a grounded wire-medium (WM) slab. Modal characteristics of mushroom structures are studied in conjunction with the surface-wave and leaky-wave propagation on WM slabs based on local and nonlocal homogenization models, showing the importance of spatial dispersion (SD) in WM. It is shown that mushroom structures support proper real (bound) forward and backward modes, whose dispersion determines the stopband properties of the mushroom structure, and proper (exponentially decaying from the surface) and improper (exponentially growing from the surface) complex leaky-wave modes related to the backward and forward radiation, respectively. Results obtained by different homogenization models are compared leading to important conclusions. Specifically, an interesting observation concerns the mushroom structures with short vias, wherein the SD of the WM slab is significantly reduced, and the results of local and nonlocal homogenization models are in excellent agreement.**

***Index Terms*—Analytical modeling, electromagnetic-bandgap (EBG) structures, high-impedance surfaces (HIS), homogenization, leaky waves, mushroom structures, spatial dispersion (SD), surface waves, wire medium (WM).**

I. Introduction

PERIODIC surfaces acting as frequency selective surfaces (FSSs) have been of interest for a long time due to their broad applications in microwave and millimeter-wave technologies [1]. In recent years, there has been a growing demand in the development of artificial periodic impedance surfaces for the realization of high-impedance surface (HIS) structures composed of FSS elements printed on a grounded dielectric slab. This includes patch arrays with grounding vias (mushroom-type structures) [2]–[4], patch arrays without vias [5]–[7], printed dipole/slot arrays [8], [9], dipole/slot arrays of different resonant length in order to achieve a multiband response [10], [11], and more complicated configurations of unit cells [12], among others. HIS structures have been used as substrates in low-profile antennas in order to improve matching and radiation antenna characteristics and minimize mutual coupling between antennas [13], [14], hard walls in the TEM waveguides [9], [15]–[17], absorbers [18], [19], and in planar tunable reflect-arrays [20], [21].

It is well known that HIS structures possess the electromagnetic-bandgap (EBG) properties (associated with a stopband for surface-wave propagation) and the artificial magnetic conductor (AMC) properties (related to the reflection phase characteristics of the surface, typically when the reflection phase varies in between $+90^\circ$ and -90°). However, in general, the EBG and AMC frequency bands of printed HIS structures do not coincide [6] (in particular, for HIS structures without vias). This is related to the fact that the stopband for surface waves occurs at the guided wavelengths of proper complex modes equal to a double period of the FSS grid [22], which is associated with the Bragg diffraction in the first Brillouin zone, but the AMC properties are due to the resonant response of the entire HIS structure (and not due to the resonance of the FSS grid by itself).

Recent trends in the miniaturization of FSS elements used in HIS structures revealed some concerns regarding the AMC and EBG properties and at the same time created possibilities for alternative modeling using the ideas from the emerging research area of metamaterials. It has been recently shown in [23]–[25] that in dense HIS structures without vias with the sub-wavelength dimensions and period of FSS elements (square patch or the Jerusalem cross), no stopband between TM and TE surface-wave modes occurs at low frequencies, wherein the HIS structure exhibits AMC properties (it should be noted that the terminology of modes for sub-wavelength periodic structures used here and throughout this paper is based on the modal classification of dielectric slab waveguides, and the modes of periodic structures are understood as perturbed modes of the back-

Manuscript received March 22, 2009; revised June 29, 2009. First published October 06, 2009; current version published November 11, 2009. This work was supported in part by the Academy of Finland under the Center-of-Excellence Program.

A. B. Yakovlev is with the Department of Electrical Engineering, The University of Mississippi, University, MS 38677-1848 USA (e-mail: yakovlev@olemiss.edu).

M. G. Silveirinha is with the Departmento de Engenharia Electrotécnica, Instituto de Telecomunicacões, Universidade de Coimbra, 3030 Coimbra, Portugal (e-mail: mario.silveirinha@co.it.pt).

O. Luukkonen, C. R. Simovski, I. S. Nefedov, and S. A. Tretyakov are with the Department of Radio Science and Engineering/SMARAD Center of Excellence, TKK Helsinki University of Technology, FI-02015 TKK, Finland (e-mail: olli.luukkonen@tkk.fi; csimovsk@cc.hut.fi; igor.nefedov@tkk.fi; sergei.tretyakov@tkk.fi).

Color versions of one or more of the figures in this paper are available online at http://ieeexplore.ieee.org.

Digital Object Identifier 10.1109/TMTT.2009.2031933

0018-9480/$26.00 © 2009 IEEE

Authorized licensed use limited to: Instituto de Telecomunicacoes. Downloaded on November 15, 2009 at 11:40 from IEEE Xplore. Restrictions apply.

ground structure within the limits of homogenization models). In this case, the AMC resonance is understood in the sense of a parallel resonance of the grid impedance of the FSS structure and the surface impedance of a grounded dielectric slab [26], which appears at low frequencies (in contrast to EBG properties at higher frequencies due to the Bragg diffraction). Unlike printed HIS structures without vias, mushroom-type HIS structures [2], [3] may have simultaneously the AMC and EBG characteristics. In fact, it has been shown in [27] and [28] that at low frequencies, wherein the mushroom structures experience the AMC properties, there is also a stopband for TE and TM surface-wave modes. It should be noted that the nature of the AMC resonance in mushroom-type structures is very much similar to that in printed HIS structures without vias (in the sense of a parallel resonance of a capacitive grid and inductive grounded dielectric slab with embedded vias). However, in contrast to the EBG properties in traditional FSS and HIS structures without vias, the stopband properties for proper surface-wave modes in mushroom-like structures are due to occurrence of TM backward leaky waves associated with the wire-medium (WM) slab and the capacitive grid.

This paper proposes a new methodology for rapid and accurate analysis of natural modes of electrically dense mushroom-type HIS structures. In this approach, mushroom structures are considered as a WM slab in conjunction with a planar printed grid of dense FSS elements (patch array or Jerusalem cross array, among others). The analysis is based on local and nonlocal homogenization models of a WM slab [21], [29] and a dynamic model of the grid (patch array [7] or Jerusalem cross array [23], [30], although the analysis of this study is limited to the case of patch array) resulting in a dispersion equation for the natural modes of mushroom-type HIS structures. Dispersion behavior of proper and improper, real and complex solutions is studied revealing interesting wave phenomena related to backward propagation, stopband characteristics for proper real modes, and backward and forward radiation associated with proper complex and improper complex leaky-wave modes. The results obtained by different homogenization models are compared, and conclusions are made regarding the physics of surface-wave and leaky-wave propagation and the importance of spatial dispersion (SD) properties of WM slabs.

Regarding the SD in wire media [31], [32], it has been shown that even for electrically thin grounded WM slabs, nonlocal methods become essential in order to accurately predict the electromagnetic response of the wire media [29], [33]–[35]. SD has also been taken into account in the analysis of eigenmodes in bounded WM structures [36]–[38] and in the study of WM slabs excited by a dipole source [39], [40]. In particular, it has been demonstrated in a recent study [29] that the WM response may be distinctively different from that of a uniaxial local material due to the effects of SD. Some ideas to reduce the effects of SD in wire media have been proposed in [41], and include coating the wires with a magnetic material or attaching large conducting structures to the wires (e.g., conducting plates). In fact, the latter strategy proposed in [41] is intrinsic to mushroom-type HIS structures composed of a WM slab connected to a grid of printed FSS elements, which was used by the authors of this paper independently of [41] for the explanation of the results obtained by local and nonlocal homogenization models [42], [43].

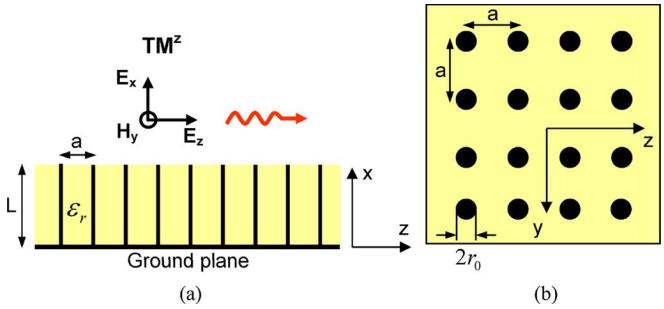

Fig. 1. Geometry of the WM slab for the analysis of TM^z surface-wave and leaky-wave propagation. (a) Side view. (b) Top view.

This paper is organized as follows. In Section II, local and nonlocal homogenization models are summarized for WM slabs, and Section III focuses on the development of nonlocal homogenization model for the analysis of the natural modes of mushroom-type HIS structures. Dispersion behavior of surface-wave and leaky-wave modes is presented in Section IV for WM slabs and mushroom HIS structures. Conclusions regarding the applicability of local and nonlocal homogenizations are drawn in Section V.

II. Homogenization of WM Slabs

In this section, we summarize the formalism of nonlocal [29] and local [21] homogenization models for the analysis of natural modes of WM slabs. The WM slab is composed of a 2-D square lattice of vertical (along the x-direction) metallic vias of radius r_0 embedded in a grounded dielectric slab of thickness L and permittivity ε_r (with the geometry shown in Fig. 1). The period of vias in the lattice is a, and it is assumed that the vias are connected to the ground plane. The WM slab may support TE^z and TM^z surface-wave modes with respect to the direction of propagation (z-direction). However, TE^z modes (with the electric field parallel to the ground) do not interact with the metallic vias and propagate as in the grounded dielectric slab. In the following analysis, we concentrate on the TM^z surface waves only. The time dependence of the form $e^{j\omega t}$ is assumed and suppressed.

A. Nonlocal Homogenization for WM Slabs

Following [29] and [32], the WM for long wavelengths (with respect to the array period) can be characterized by a spatially dispersive model of a uniaxial anisotropic material with the effective permittivity

$$\underline{\boldsymbol{\varepsilon}}_{\mathrm{eff}} = \varepsilon_0 \varepsilon_r \left(\varepsilon_{xx}(\omega, k_x)\, \hat{\mathbf{x}}\hat{\mathbf{x}} + \hat{\mathbf{y}}\hat{\mathbf{y}} + \hat{\mathbf{z}}\hat{\mathbf{z}} \right)$$
$$\varepsilon_{xx}(\omega, k_x) = 1 - \frac{k_p^2}{k_r^2 - k_x^2} \tag{1}$$

where k_p is the plasma wavenumber defined in [32, eq. (10)], $k_r = k_0\sqrt{\varepsilon_r}$ is the wavenumber in the host material, $k_0 = \omega/c$ is the wavenumber in free space, and k_x is the x-component of the wave vector $\mathbf{k}$ associated with the plane-wave modes of the unbounded medium. The dispersion equation for the TEM- and

Authorized licensed use limited to: Instituto de Telecomunicacoes. Downloaded on November 15, 2009 at 11:40 from IEEE Xplore. Restrictions apply.

TM-polarized waves in the unbounded WM can be obtained by substituting the effective permittivity (1) into Maxwell's equations, resulting in the following:

$$\left(k_r^2 - k_x^2 - k_z^2 - k_p^2\right)\left(k_x^2 - k_r^2\right) = 0 \tag{2}$$

where k_z is the z-component of the wave vector $\mathbf{k} = (k_x, 0, k_z)$. The solution of (2) gives two independent eigenwaves, where the first factor determines the dispersion properties of the TM wave and the second factor corresponds to the TEM wave. For the TEM wave, $k_r = \pm k_x$ for any k_z.

The dispersion equation for TM^z surface-wave modes of the WM slab (Fig. 1) has been derived in [29] by considering a scattering problem for an obliquely incident TM-polarized plane wave, where the poles of the reflection coefficient [29, eq. (9)] correspond to the propagation constants of surface-wave modes [29, eq. (14)]. The same dispersion equation can be derived by considering a source-free spectral problem for the natural modes of the WM slab. The magnetic field in the air region and the WM slab of the TM^z modes can be obtained as follows:

$$\begin{aligned} H_y &= Ae^{-\gamma_0(x-L)}e^{-jk_z z}, \qquad \text{for } x > L \\ H_y &= \left(B_{\mathrm{TEM}}\cos\left(k_{\mathrm{TEM}}x\right) + B_{\mathrm{TM}}\cosh\left(\gamma_{\mathrm{TM}}x\right)\right)e^{-jk_z z}, \\ &\qquad \text{for } 0 < x < L \end{aligned} \tag{3}$$

where the boundary condition on the perfect electric conductor (PEC) ground plane at $x = 0$ has been satisfied. In (3), A, B_{TEM}, and B_{TM} are the amplitude coefficients of TM^z natural modes with the propagation constant $k_z = \mathrm{Re}\{k_z\} + j\mathrm{Im}\{k_z\}$, $\mathrm{Im}\{k_z\} \leq 0$; $\gamma_{\mathrm{TM}} = \sqrt{k_z^2 + k_p^2 - k_r^2}$, $\gamma_0 = \sqrt{k_z^2 - k_0^2}$, and $k_{\mathrm{TEM}} = k_r$. The total field of surface waves in the WM slab region is obtained as a combined contribution of TEM and TM fields having different wave vectors such that for proper (bound) surface waves the wave vector of the TEM field is real-valued and the wave vector of the TM field is complex-valued (the TM part of the surface-wave modes in the WM slab is typically strongly confined to the air–slab interface, especially for long wires). Enforcing the continuity of tangential electric and magnetic fields at the air–dielectric interface and an additional boundary condition (ABC) at the air–slab (WM) interface at $x = L$ (given in terms of the H_y-component of the magnetic field in (6), [29]), the dispersion equation for TM^z natural modes is obtained as follows:

$$\begin{aligned} k_{\mathrm{TEM}}k_p^2\tan\left(k_{\mathrm{TEM}}L\right) - k_z^2\gamma_{\mathrm{TM}}\tanh\left(\gamma_{\mathrm{TM}}L\right) \\ -\varepsilon_r\gamma_0\left(k_p^2 + k_z^2\right) = 0 \end{aligned} \tag{4}$$

which is the same as [29, eq. (14)], except for the propagation constant in the radial direction that was defined in [29] as $k_{||} = \sqrt{k_y^2 + k_z^2}$. The factor γ_0 induces branch points in the complex k_z-plane at $k_z = \pm k_0$. Proper modes (above cutoff) reside on the proper Riemann sheet with the field decaying in the x-direction as $e^{-\gamma_0 x}$, where $\mathrm{Re}\{\gamma_0\} > 0$, and improper modes (below cutoff) reside on the improper Riemann sheet where $\mathrm{Re}\{\gamma_0\} < 0$ (with the field growing in the x-direction). Branch cuts that separate proper and improper Riemann sheets are defined by $\mathrm{Re}\{\gamma_0\} = 0$, leading to the hyperbolic branch cuts

$$\mathrm{Im}\{k_z\} = \frac{\mathrm{Im}\{k_0\}\mathrm{Re}\{k_0\}}{\mathrm{Re}\{k_z\}}, \qquad |\mathrm{Re}\{k_z\}| < |\mathrm{Re}\{k_0\}|. \tag{5}$$

It should be noted that the nonlocal homogenization model of the WM slab takes into account SD by considering a combined contribution of TEM and TM fields and requires an ABC at the air–WM slab interface, and it is referred here to as the *SD+ABC* model. The ABC enables the accurate modeling of the physical behavior of the current along the vias at the air–WM slab interface and at the connection of vias to the PEC ground plane, which is equivalent to the following conditions for the microscopic current $I(x)$: $I(x)|_{x=L^-} = 0$ (which corresponds to the maximum charge accumulated on the tips of the vias) and $dI(x)/dx|_{x=0^+} = 0$ (associated with zero charge density at the connection of vias to the ground plane).

B. Local Homogenization of WM Slabs

A local model of the WM slab (Fig. 1) has been introduced in [21] and [26] as a quasi-static approximation of a uniaxial anisotropic material composed of infinitely long wires and characterized by the effective permittivity (1) with the normal component defined by the Drude model without considering SD effects

$$\varepsilon_{xx}(\omega) = 1 - \frac{k_p^2}{k_r^2}. \tag{6}$$

Thus, the proposed local model treats the WM as an epsilon-negative (ENG) material below the plasma frequency. It should be noted that the local model of a WM slab, referred here to as the *ENG approximation*, has been used in [21] in conjunction with a patch array grid in order to develop a local model for mushroom HIS structures.

The surface impedance of a WM slab with vias connected to the PEC ground plane (Fig. 1) "seen" by TM^z natural modes can be written as follows [21]:

$$Z_{wm}(\omega, k_z) = j\omega\mu_0\frac{\tanh(\gamma L)}{\gamma}\frac{k_r^2 - k_p^2 - k_z^2}{k_r^2 - k_p^2} \tag{7}$$

where γ is the propagation constant in the WM slab in the normal direction (x-direction)

$$\gamma = \sqrt{\frac{k_z^2}{\varepsilon_{xx}} - k_r^2} \tag{8}$$

and k_p is the quasi-static approximation of the plasma wavenumber given in [21, eq. (6)] and [26]. It should be noted that at the plasma frequency, the normal component of the effective permittivity ε_{xx}, defined by the ENG approximation (6), crosses zero, resulting in a singularity in (8). In this regime, the local model predicts that the WM slab supports multiple spurious higher order surface-wave and leaky-wave modes in a very narrow frequency range close to the plasma frequency, which, as will be discussed further in Section IV, are not observed in the real structured substrate. These spurious solutions may possibly be eliminated from the modal spectrum,

Authorized licensed use limited to: Instituto de Telecomunicacoes. Downloaded on November 15, 2009 at 11:40 from IEEE Xplore. Restrictions apply.

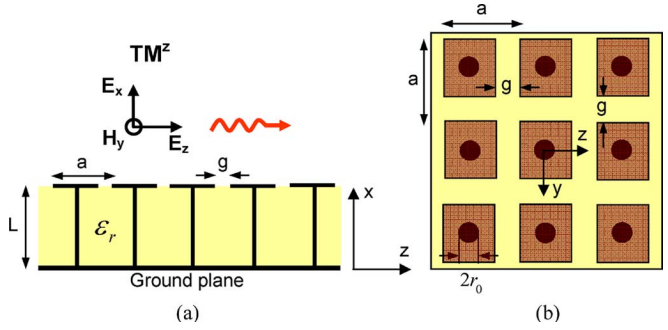

Fig. 2. Geometry of the mushroom-type HIS structure for the analysis of TM_z surface-wave and leaky-wave propagation. (a) Side view. (b) Top view.

or at least may be significantly damped, by introducing small losses in the dielectric permittivity of the host material ε_r.

The spectral problem is equivalent to the analysis of the natural modes supported by the impedance surface (7) (with the assumption that there is no field beyond the impedance surface), resulting in the dispersion equation for TM^z surface-wave and leaky-wave modes [26]

$$k_z = k_0\sqrt{1-\left(\frac{Z_{wm}}{\eta_0}\right)^2} \tag{9}$$

where $\eta_0 = \sqrt{\mu_0/\varepsilon_0}$ is the characteristic impedance of free space. It should be noted that $Z_{wm} = Z_{wm}(\omega, k_z)$, and (9) is the implicit form of the dispersion equation for the natural modes, which can be solved numerically for the propagation constant k_z.

III. Homogenization of Mushroom-Type HIS Structures

In this section, we present the analysis of the natural modes of mushroom-type HIS structures based on nonlocal and local homogenization models. Mushroom structures are formed by a grid of FSS elements (patches, Jerusalem crosses, etc.) printed on a grounded dielectric slab with metallic pins connected to the grid and to the ground (with the geometry shown in Fig. 2 for the specific case of a patch array). In Fig. 2, a is the period in the 2-D square lattice (which is the same for the grid and the WM) and g is the gap between the adjacent grid elements. As in the case of a WM slab, mushroom-type HIS structures support TE^z and TM^z surface-wave modes as natural modes of these periodic structures. The analysis is limited here to TM^z modes because TE^z surface waves do not interact with the vias and propagate as in the HIS structure formed by a metallic grid printed on a grounded dielectric slab [23]–[25]. The proposed methodology considers mushroom structures as sub-wavelength FSS grids printed on a WM slab, and the material presented in Section II is essential for the characterization of the spectrum of natural modes of mushroom structures based on nonlocal and local homogenizations.

A. Nonlocal Homogenization for Mushroom Structures

Considering a source-free spectral problem for the TM^z natural modes of the mushroom structure (Fig. 2) and following the formalism presented in Section II for the WM slab (Fig. 1), the magnetic field in the air region and WM slab can be represented in form (3), subject to the two-sided impedance boundary condition at the grid interface ($x = L$)

$$E_z = Z_g\left(H_y|_{x=L^+} - H_y|_{x=L^-}\right) \tag{10}$$

with the E_z-component of the electric field being continuous across the grid such that $E_z = (1/j\omega\varepsilon_0\varepsilon(x))(dH_y/dx)$ is continuous, resulting in

$$E_z|_{x=L^-} = E_z|_{x=L^+} \tag{11}$$

which is equivalent to the following condition for the magnetic field:

$$\frac{1}{\varepsilon_r}\frac{dH_y}{dx}|_{x=L^-} = \frac{dH_y}{dx}|_{x=L^+}. \tag{12}$$

Here,

$$\varepsilon(x) = \begin{cases} 1, & x > L \\ \varepsilon_r, & 0 < x < L. \end{cases}$$

In (10), Z_g is the effective surface impedance of the grid "seen" by the TM^z natural modes. Analytical dynamic models for the grid impedance have been obtained in terms of effective circuit parameters for sub-wavelength printed arrays realized by various FSS elements (with the period much smaller than the effective wavelength), including strips and patches [7], Jerusalem crosses [23], [30], and cross dipoles [44], among others. For the sake of brevity, we present here only the expression for the surface impedance of the grid comprising square patches (the case of the TM polarization), which is obtained by first considering a strip mesh with square holes and then applying the approximate Babinet principle, resulting in the capacitive grid impedance of the complementary structure (i.e., array of patches) [7]

$$Z_g = -j\frac{\eta_{\text{eff}}}{2\alpha} \tag{13}$$

where $\eta_{\text{eff}} = \eta_0/\sqrt{\varepsilon_{\text{eff}}}, \varepsilon_{\text{eff}} = (\varepsilon_r + 1)/2$, and α is the grid parameter

$$\alpha = \frac{k_{\text{eff}}a}{\pi}\ln\left(\sin^{-1}\left(\frac{\pi g}{2a}\right)\right). \tag{14}$$

To complete the formulation, an ABC is required at the connection of vias to the grid $x = L^-$, as well as at the connection of vias to the ground plane $x = 0^+$. Assuming that the patches are wide enough, we use the same condition as in [35] at the connection of the vias to both the infinite ground plane and the patches

$$\frac{d}{dx}\left(\omega\varepsilon_0\varepsilon_r\hat{\mathbf{x}}\cdot\mathbf{E} + (\hat{\mathbf{x}}\times\hat{\mathbf{z}}k_z)\cdot\mathbf{H}\right) = 0. \tag{15}$$

This leads to the following condition in terms of field components:

$$k_0\varepsilon_r\frac{dE_x}{dx} - k_z\eta_0\frac{dH_y}{dx} = 0. \tag{16}$$

Authorized licensed use limited to: Instituto de Telecomunicacoes. Downloaded on November 15, 2009 at 11:40 from IEEE Xplore. Restrictions apply.

For the unbounded WM from Ampere's circuital law, we obtain

$$E_x = -\frac{\eta_0}{jk_0\varepsilon_r\varepsilon_{xx}(k_x)}\frac{dH_y}{dz} = \frac{k_z\eta_0}{k_0\varepsilon_r\varepsilon_{xx}(k_x)}H_y \tag{17}$$

where the normal component of the effective permittivity $\varepsilon_{xx}(k_x)$ is defined by (1) such that for the TM fields [29]

$$\varepsilon_{xx}\left(k_r^2 = k_p^2 + k^2\right) \equiv \varepsilon_{xx}^{\mathrm{TM}} = 1 - \frac{k_p^2}{k_z^2 + k_p^2} \tag{18}$$

with $k^2 = \mathbf{k}\cdot\mathbf{k}$. Then, using (3) together with (17) and (18), the E_x-component of the electric field in the region below the grid ($0 < x < L$) can be obtained as follows:

$$E_x = \frac{k_z\eta_0}{k_0\varepsilon_r\varepsilon_{xx}^{\mathrm{TM}}}B_{\mathrm{TM}}\cosh\left(\gamma_{\mathrm{TM}}x\right)e^{-jk_zz}. \tag{19}$$

The dispersion equation for TM^z surface-wave and leaky-wave modes is obtained by enforcing the boundary conditions (10) and (12) for the tangential magnetic fields (3) at the grid interface $x = L$ and the ABC condition (16) together with (19) at the connection of vias to the grid $x = L^-$ and to the ground at $x = 0^+$, leading to

$$\frac{\varepsilon_r\varepsilon_{xx}^{\mathrm{TM}}}{\gamma_{\mathrm{TM}}}\coth\left(\gamma_{\mathrm{TM}}L\right) - \frac{\varepsilon_r\left(1-\varepsilon_{xx}^{\mathrm{TM}}\right)}{k_{\mathrm{TEM}}}\cot\left(k_{\mathrm{TEM}}L\right) + \left(\frac{1}{\gamma_0} - j\frac{\eta_0}{Z_gk_0}\right) = 0. \tag{20}$$

Here, the wavenumber γ_0 induces branch points in the complex k_z-plane at $k_z = \pm k_0$, separating proper (above cutoff) and improper (below cutoff) modes defined on the corresponding Riemann sheets.

As in the case of the WM slab, the nonlocal homogenization model of the mushroom structures takes into account SD effects of WM and requires the use of ABCs at the interfaces, and it is referred here to as the *SD+ABC* model. The physical behavior of the current at the connection points is accurately enforced by the ABC, which can be written for the microscopic current $I(x)$ as follows: $dI(x)/dx|_{x=L^-} = 0$ and $dI(x)/dx|_{x=0^+} = 0$. It can be shown that the microscopic current along the vias can be expressed in terms of the averaged (macroscopic) fields of 2-D square lattice of mushrooms [35]

$$I(x) = -ja^2\left(\omega\varepsilon_0\varepsilon_rE_x - k_zH_y\right). \tag{21}$$

B. Local Homogenization for Mushroom Structures

A local homogenization of mushroom-type HIS structures with electrically short vias is based on the ENG approximation of the WM slab (the local model described in Section II) and a dynamic model of the grid characterized by the surface impedance in terms of effective circuit parameters [21]. It does not take into account SD effects in the WM and does not require an ABC at the interfaces. The dispersion equation for the TM^z natural waves is obtained by considering the equivalent surface impedance Z_s of the mushroom HIS structure (Fig. 2), which is given by the parallel connection of the surface impedance of the grid Z_g and the surface impedance of the WM slab Z_{wm} [26]

$$Z_s = \frac{Z_gZ_{wm}}{Z_g + Z_{wm}}. \tag{22}$$

In (22), Z_{wm} is given by (7), which is obtained using the ENG approximation (local model), and Z_g represents the surface impedance of the homogenized grid "seen" by the TM^z natural modes; in particular, for the patch array, Z_g is given by (13) and (14), [7].

The spectral problem for the natural modes of mushroom structure is then equivalent to the analysis of the natural modes of the impedance surface described by Z_s [defined by (22)] (with no field beyond the impedance surface), resulting in the dispersion equation for the TM^z surface-wave and leaky-wave modes (similar to (9) for the WM slab with Z_{wm} replaced by Z_s)

$$k_z = k_0\sqrt{1 - \left(\frac{Z_s}{\eta_0}\right)^2} \tag{23}$$

where $Z_s \equiv Z_s\left(\omega, k_z\right)$. The dispersion (23) can be solved numerically for the propagation constant k_z.

It should be noted that the local model does not require any boundary conditions at the connection of the vias to the metallic interfaces (grid elements and ground plane); however, it is essential that in the physical configuration (realistic structures), the vias are connected to the grid and the ground plane and the current is continuous at the interfaces. In general, the local model will fail (the reason will be clear in Section IV) if the vias are not connected to the grid, e.g., in the case of a grid complementary to the patch array, i.e., a strip mesh with square holes.

IV. Numerical Results and Discussion

In this section, based on the proposed nonlocal and local homogenization models, the dispersion behavior of TM^z surface-wave and leaky-wave modes is studied in the WM slabs and mushroom-type HIS structures.

A. Surface Waves and Leaky Waves on WM Slabs

1) WM Slabs With Long Vias: We begin with the analysis of the modal properties of the WM slab with electrically long vias (Fig. 1). In the first example, the WM slab with long vias has the following parameters: $a = 1$ mm, $L = 5$ mm, $r_0 = 0.05$ mm, and $\varepsilon_r = 1$. The dispersion behavior of the proper real (bound) and improper real surface-wave modes based on the SD+ABC model [as the numerical solution of the dispersion equation (4)] is shown in Fig. 3 as the normalized propagation constant k_z/k_0 versus the normalized frequency $L/\lambda_0/(4\sqrt{\varepsilon_r})$ (for the case of $\varepsilon_r = 1$). Two proper TM^z surface-wave modes are shown, and the dispersion behavior agrees very well with the HFSS results [45]. At low frequencies, k_z/k_0 is close to 1, indicating that the surface wave weakly interacts with the WM and propagates primarily in the air region with the field exponentially decaying in the vertical direction (with the factor $e^{-\gamma_0x}, \mathrm{Re}\{\gamma_0\} > 0$) as the proper real (bound) mode. With the increase of frequency, the surface wave interacts more strongly with the WM resulting

Authorized licensed use limited to: Instituto de Telecomunicacoes. Downloaded on November 15, 2009 at 11:40 from IEEE Xplore. Restrictions apply.

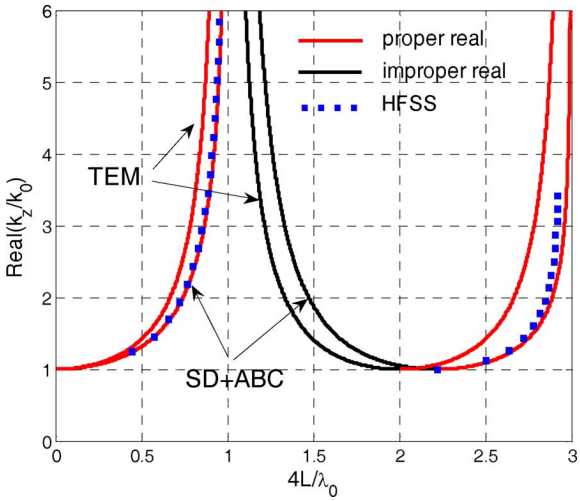

Fig. 3. Dispersion behavior of TM^z surface-wave modes in the WM slab with long vias based on the SD+ABC homogenization model and the TEM approximation.

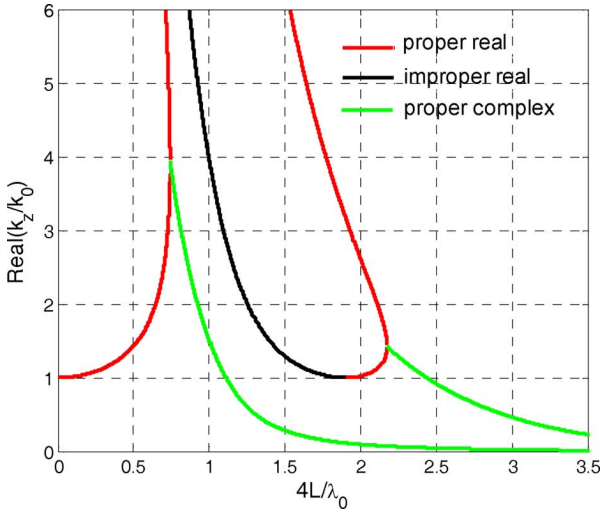

Fig. 4. Dispersion behavior of TM^z surface-wave and leaky-wave modes in the WM slab with long vias based on the ENG model. The ENG results are qualitatively different from those obtained by the SD+ABC model and the TEM approximation shown in Fig. 3.

in an increase of the propagation constant, where the dispersion properties of the TM^z surface wave are determined by the combined contributions of the TEM and TM fields in the WM slab. At the frequency around 15 GHz corresponding to $L = \lambda_0/(4\sqrt{\varepsilon_r})$, a stopband occurs for the first TM^z surface-wave mode, and at the frequency for which $L = 3\lambda_0/(4\sqrt{\varepsilon_r})$ (corresponding to 45 GHz) there is a stopband for the second TM^z mode [29].

The stopbands for the proper modes shown in Fig. 3 are at low frequencies within the limits of the homogenization model for the WM slab (with the plasma frequency $f_p/\sqrt{\varepsilon_r}$ at 92.13 GHz). The nature of stopbands in the WM slab at low frequencies is similar to that found in traditional FSS structures at high frequencies (referred to as closed stopbands) [22]. The homogenization for surface waves requires that $k_z a \ll \pi$, which defines a low-frequency range close to the left hyperbola in the first Brillouin zone. The first and second stopbands in Fig. 3 occur exactly at $k_z a = \pi$ associated with the Bragg diffraction limit in the first Brillouin zone. Even though the homogenization model cannot accurately predict the wave behavior at the stopband frequency (since the concept of Bragg diffraction is not applicable for a continuous material, and consequently homogenization does not impose any bound on k_z when approaching the stopband frequency), the general agreement between analytical and the numerical solutions in the vicinity of the stopband is good, especially for the SD+ABC homogenization model. This somewhat surprising result is partially explained by the fact that the dispersion characteristic of the TEM mode, $k_{\mathrm{TEM}} = k_r$, is *exact*, i.e., it is valid for arbitrarily large frequencies and phase shifts between currents in vias. Quite differently, the dispersion characteristic of the TM mode is only valid in the long-wavelength limit. However, as discussed below, the contribution of the TM mode to the fields in the WM slab may be residual, and due to this reason, the homogenization model may still be pretty accurate even beyond the usual homogenization bounds ($k_z a \ll \pi$ and $k_0\sqrt{\varepsilon_r} a \ll \pi$). In order to demonstrate this property, we show in Fig. 3 the results obtained in the TEM approximation when the field in the WM slab region is defined by the TEM mode only (see (3) with the TM field set to zero, [29]). This means that only the TEM mode contributes to the field of the TM^z surface-wave modes of the WM slab. It can be seen that the overall behavior of proper and improper real solutions is captured by the TEM approximation (even for the second mode), and, therefore, the TEM mode has the dominant contribution to the field of TM^z surface waves (in comparison with the TM part in (3), which attenuates rapidly away from the air–WM slab interface).

The results of the ENG approximation [obtained using (9)] are shown in Fig. 4 for the same example of the WM slab with long vias. It can be seen that the ENG model results agree with the SD+ABC and the TEM approximation results only at low frequencies, and with the increase of frequency, the dispersion behavior of surface waves becomes very different from that shown in Fig. 3. The ENG model predicts proper real and proper complex backward waves (with the group velocity in the $-z$-direction as the negative slope of dispersion curves of the corresponding modes). In this example of a WM slab with long vias, the ENG model fails even at low frequencies far away from the plasma frequency of 92.13 GHz.

For densely packed vias with the period of the lattice a reduced, the dispersion behavior of TM^z surface-wave proper real (bound) modes based on the SD+ABC model is almost unaffected, as it is shown in Fig. 5. In fact, for a small a ($a \ll L$), the SD+ABC results approach the TEM approximation results, when the surface waves "see" the WM slab as a material with extreme anisotropy [29].

The SD+ABC model also predicts proper complex and improper complex leaky-wave modes in the WM slab with long vias, as is shown in Fig. 6. Starting with the small period ($a =$ 1 mm), a proper complex backward mode with a large attenuation constant [see Fig. 6(b)] is found. This mode is significantly affected by the increase of the lattice period. For the cases reported in Fig. 6 (with $a = 3$ mm and $a = 5$ mm), the pole of proper complex mode migrates from the first quadrant of the

Authorized licensed use limited to: Instituto de Telecomunicacoes. Downloaded on November 15, 2009 at 11:40 from IEEE Xplore. Restrictions apply.

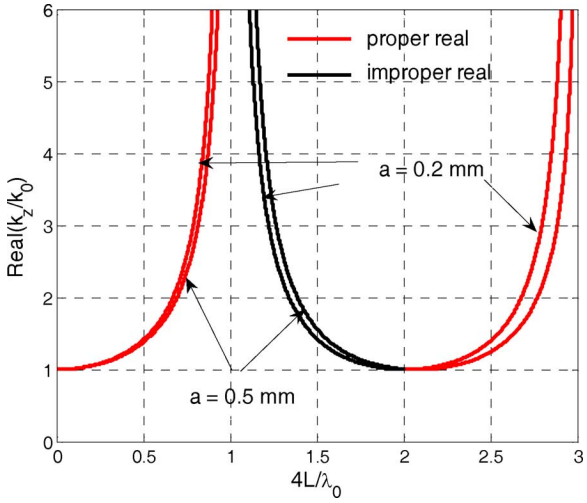

Fig. 5. Dispersion behavior of surface waves on WM slab with highly-dense long vias based on the SD+ABC model. The modal behavior is almost unaffected by altering the period of vias in the lattice.

complex propagation constant plane into the second quadrant by crossing the Sommerfeld branch cut and becomes the improper complex forward mode propagating in the negative z-direction. It can be seen in Fig. 6 that the improper complex leaky wave remains physical ($-1 < \mathrm{Re}\{k_z/k_0\} < 0$) in the shown frequency range with a very small attenuation constant.

The dispersion behavior based on the ENG model is significantly affected by altering the period of vias. In Fig. 7 for the period of vias 0.2 mm, the behavior of the first TM^z surface wave is very similar to that predicted by the SD+ABC model, and the leaky-wave cutoff of the first proper complex mode is pushed toward higher values of the propagation constant. The second mode (real and complex regimes) is also significantly deformed. It can be seen (Fig. 7) that the dispersion behavior of proper real (bound) modes based on the ENG model for highly packed vias is close to the modal behavior obtained by the SD+ABC model and the TEM approximation. Thus, we conclude that the ENG model describes adequately the physics of surface-wave propagation only in highly dense WM slabs, when the normal permittivity ε_{xx} defined by (6) is very large and negative (or equivalently when the frequency of operation is much smaller than the plasma frequency; notice that the plasma frequency for highly packed vias is pushed to hundreds of gigahertz). In this sense, the ENG and TEM approximation results agree—both models have the same physical interpretation of surface-wave propagation in a medium with extreme anisotropy, with the component of the permittivity along the direction of the wires, such that $|\varepsilon| \gg 1$. It should be noted that the leaky waves shown in Fig. 4 based on the ENG approximation do not accurately describe the dynamics of the leaky modes of the WM slab. However, for a WM slab with highly dense vias, the leaky-wave behavior at low frequencies presented in Fig. 7 based on the ENG model is close to that obtained with the SD+ABC model (even though this mode is not physical due to a large attenuation constant). The physical leaky waves with small attenuation constant obtained with the SD+ABC model become significant only when the period is relatively large (comparable to the length of vias), as is shown in Fig. 6.

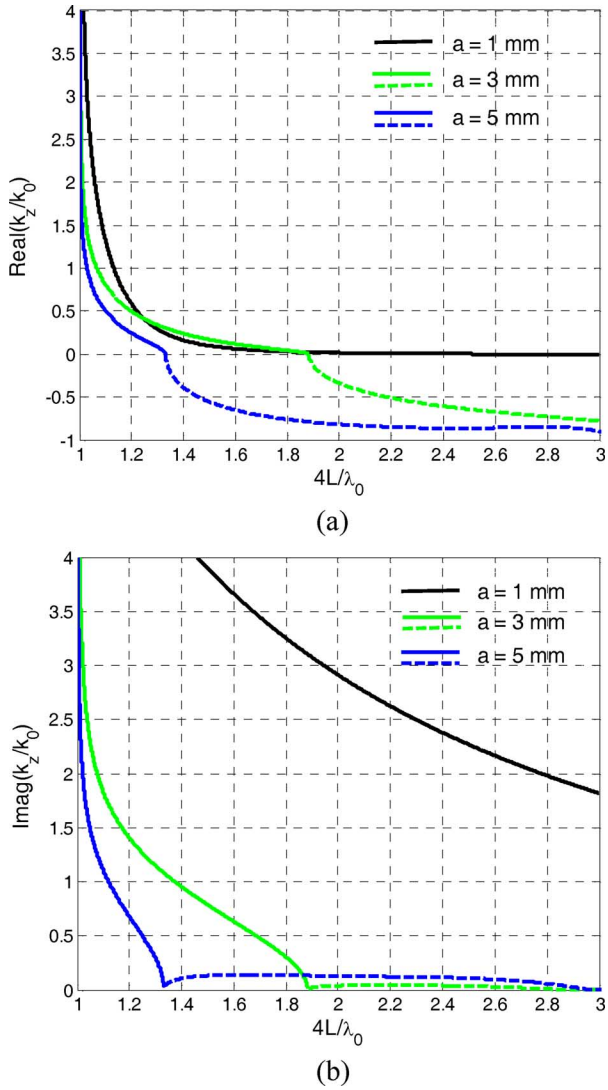

Fig. 6. Dispersion behavior of proper complex (solid line) and improper complex (dashed line) leaky-wave modes in the WM slab with long vias based on the SD+ABC model. (a) Real part of the normalized propagation constant. (b) Imaginary part of the normalized propagation constant. The modal behavior is significantly affected by increasing the period of vias in the lattice.

2) WM Slabs With Short Vias: In the second example, a WM slab with short vias (with the geometry shown in Fig. 1) is considered with the following parameters: $a = 2$ mm, $L = 1$ mm, $r_0 = 0.05$ mm, and $\varepsilon_r = 10.2$. The dispersion behavior of the first two TM^z surface-wave proper (bound) modes based on the SD+ABC model is shown in Fig. 8 as the normalized propagation constant k_z/k_0 versus frequency, and compared with the full-wave results obtained by HFSS demonstrating a good agreement, especially for the first mode.

It should be noted that in this example of short vias with a high permittivity host material, the stopband of the first TM^z mode occurs at approximately 22.8 GHz (based on High Frequency Structure Simulator (HFSS) results), which corresponds to the Bragg condition in the first Brillouin zone where $k_z a = \pi$ (with $k_z/k_0 = 3.29$). It should also be noted that, in this example, the stopband is beyond the limits of homogenization where $k_0\sqrt{\varepsilon_r}a \ll \pi$, [29], and the plasma frequency $f_p/\sqrt{\varepsilon_r}$ is 12.14 GHz. In comparison with the previous example of long

Authorized licensed use limited to: Instituto de Telecomunicacoes. Downloaded on November 15, 2009 at 11:40 from IEEE Xplore. Restrictions apply.

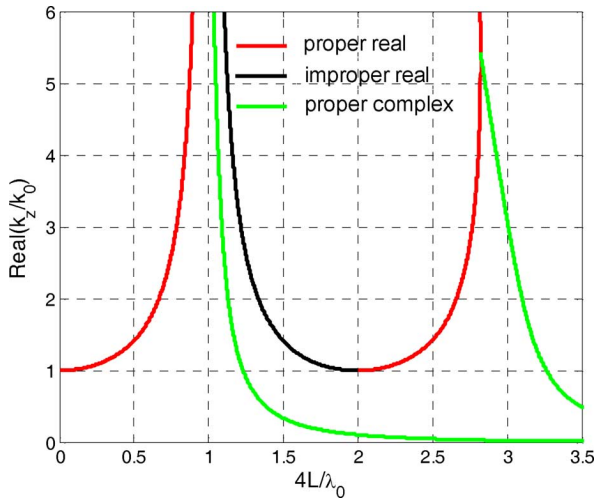

Fig. 7. Dispersion behavior of surface and leaky waves on WM slab with highly dense long vias based on the ENG model with the lattice period of $a = 0.2$ mm. The modal behavior depends significantly on the period of the vias. The surface waves propagate as in a medium with extreme anisotropy.

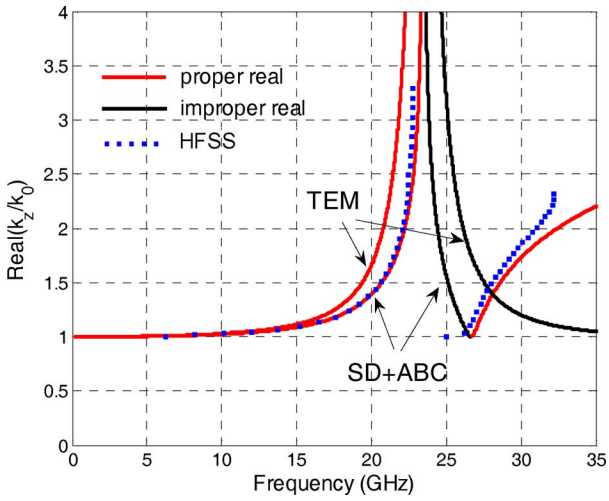

Fig. 8. Dispersion behavior of TM^z surface-wave modes in the WM slab with short vias based on the SD+ABC homogenization model and the TEM approximation.

vias, wherein the stopband of the first TM^z mode occurs at the Bragg condition, but at low frequencies with $k_0\sqrt{\varepsilon_r}a \ll \pi$, in the case of short vias, the stopband of the first mode is at high frequencies. Surprisingly, the homogenization model (SD+ABC) captures very accurately the physics in the vicinity of the stopband even beyond the homogenization limit. As discussed before, this unusual property may be partially justified by the fact that the dispersion characteristic of the TEM mode is not constrained by the usual homogenization bounds. In Fig. 8, the TEM approximation results are also shown, indicating a good agreement with the SD+ABC results at low frequencies and even above the plasma frequency; however, with the increase of frequency, the results obtained by the two models start to differ, especially for the second TM^z mode (where the TEM approximation at high frequencies above the first stopband fails).

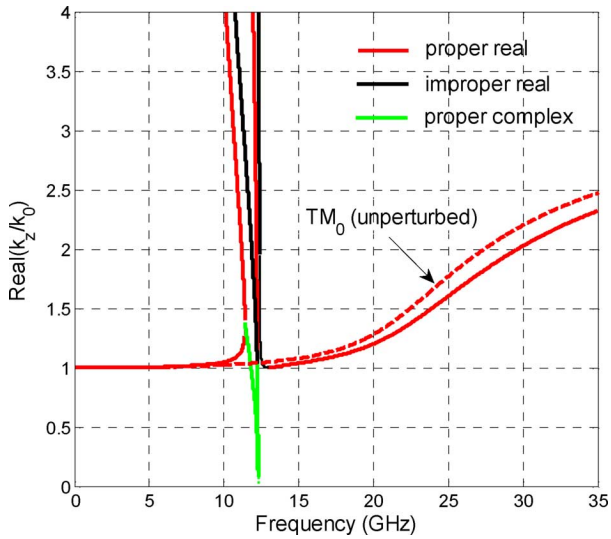

Fig. 9. Dispersion behavior of TM^z surface-wave and leaky-wave modes in the WM slab with short vias based on the ENG model. The ENG model predicts the backward and complex solutions (with dispersion significantly different from that of the modes of the actual WM slab), and spurious higher order modes in the vicinity of the plasma frequency.

The results of the TM^z surface and leaky waves on the WM slab with short vias based on the ENG model are shown in Fig. 9. It can be seen that the dispersion behavior is very different from that obtained by the SD+ABC model, except for frequencies well below the plasma frequency of 12.14 GHz. In the vicinity of the plasma frequency and above, the ENG approximation fails. Near the plasma frequency, the ENG model predicts backward and complex modes, which do not capture accurately the physics of the actual WM slab. In addition, because of the singularity in (8) where the normal permittivity $\varepsilon_{xx} = 0$ at the plasma frequency, higher order spurious real and complex modes occur (as shown in Fig. 9), which have to be discarded from the modal spectrum. Also, for comparison, the dispersion curve of the TM_0 surface wave of the grounded dielectric slab is shown, which is close to the dispersion behavior based on the ENG model, except for the narrow frequency range close to the plasma frequency.

As in the case of long vias, the dispersion behavior of surface waves in the case of short vias is almost unaffected by reducing the period of the lattice a. This is demonstrated in Fig. 10 obtained with the SD+ABC homogenization model.

However, the modal behavior of proper complex and improper complex leaky-wave modes found in the WM slab is significantly affected by varying the lattice period, as is shown in Fig. 11. As in the case of a WM slab with long vias, within the frequency range shown in Fig. 11 there is a proper complex backward leaky wave above 23.48 GHz with a large attenuation constant [see Fig. 11(b)]. With the increase of period, this mode is significantly deformed such that at some frequency the pole of the proper complex backward mode in the first quadrant of the complex propagation constant plane migrates into the second quadrant by crossing the Sommerfeld branch cut and becomes an improper complex leaky-wave mode propagating in the negative z-direction. Specifically, this transition occurs at a frequency of approximately 26.42 GHz for the case of

Authorized licensed use limited to: Instituto de Telecomunicacoes. Downloaded on November 15, 2009 at 11:40 from IEEE Xplore. Restrictions apply.

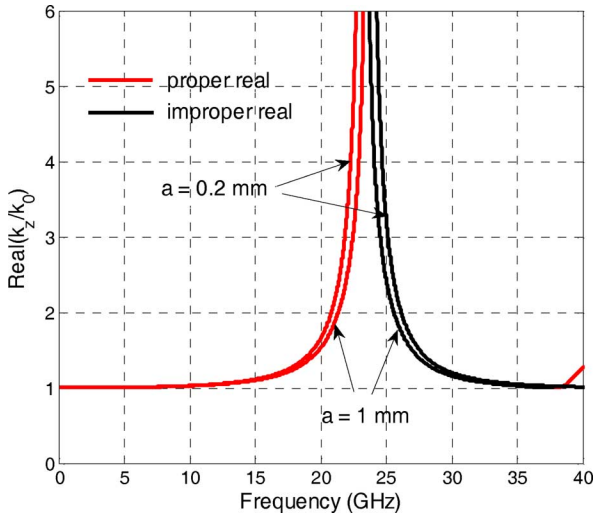

Fig. 10. Dispersion behavior of surface waves on WM slab with highly dense short vias based on the SD+ABC model. The modal behavior is almost unaffected by altering the period of vias in the lattice.

$a = 2$ mm and at a frequency of approximately 24.63 GHz for the case of $a = 3$ mm. At low frequencies below 23.45 GHz, there is also an improper complex leaky-wave mode with a large attenuation constant (this mode attenuates very rapidly before radiating).

The ENG model results depend significantly on the period of vias, as shown in Fig. 12. Specifically in Fig. 12, as the period is reduced, the leaky-wave cutoff frequencies of the proper complex modes are pushed to larger values of the propagation constant (as well as proper backward modes), and for a small period, $a = 0.2$ mm, the dispersion behavior looks very similar to that based on the SD+ABC model and the TEM approximation. This indicates that the ENG model is valid only for a highly dense WM, understood as a medium with extreme anisotropy.

These properties can be understood by noting that, in general, the nonlocal dielectric function [see (1)] may be equivalent to the local dielectric function [see (6)] in the following two different scenarios.

- The first case is when both the local and nonlocal models predict that the WM behaves as a material with extreme anisotropy $|\varepsilon_{xx}| \gg 1$. This situation occurs either for very low frequencies or when the vias are densely packed, $a/L \ll 1$ (but not necessarily electrically short) so that the plasma frequency is extremely large.
- The second case for which SD may be suppressed is when the fields in the WM slab are nearly uniform along the direction of the vias so that $d/dx \approx 0$, or equivalently, in the spectral domain, $k_x \approx 0$. Under these conditions, the dielectric function of the nonlocal model [see (1)] reduces to the dielectric function of the local model [see (6)]. This situation (i.e., $d/dx \approx 0$) requires that the current along the wires is approximately uniform in the WM slab.

It is clear that in a grounded WM slab (with no FSS grid) only the first case may be observed, i.e., the effects of SD may be suppressed only when the WM is characterized by extreme anisotropy. Indeed, the absence of the metallic grid precludes that the current along the vias is constant, as required by the

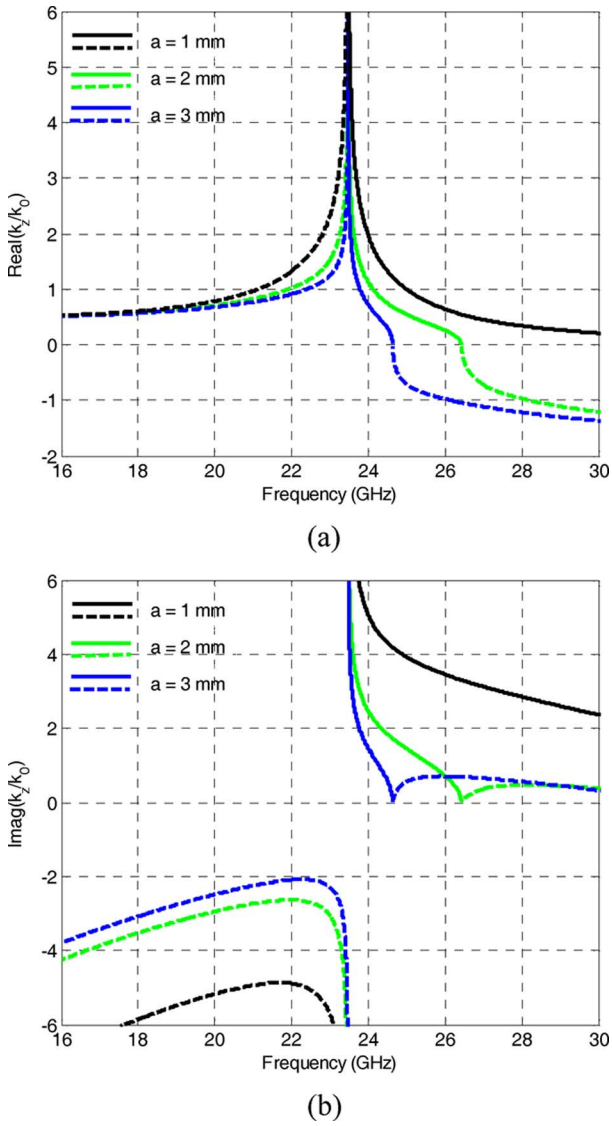

Fig. 11. Dispersion behavior of proper complex (solid line) and improper complex (dashed line) leaky-wave modes in the WM slab with short vias based on SD+ABC model. (a) Real part of the normalized propagation constant. (b) Imaginary part of the normalized propagation constant. The modal behavior is significantly affected by the period of the vias in the lattice.

second scenario. In fact, in the absence of the metallic grid, the microscopic current along the metallic wires is highly nonuniform, even for long wavelengths. To illustrate this, we plot in Fig. 13 the normalized current profile along a generic wire for the first proper real TM^z surface-wave mode in a metamaterial slab with the same parameters as in Fig. 8. The solid and dashed curves were calculated using homogenization theory [see (21)], whereas the discrete symbols were calculated using the commercial full-wave simulator CST Microwave Studio [46]. It can be seen that the current along the metallic vias varies significantly along x, and vanishes at the interface with air. Such behavior confirms that, in a grounded WM slab, the SD effects may be suppressed only when the metamaterial is characterized by extreme anisotropy, $|\varepsilon_{xx}| \gg 1$.

In summary, the inclusion of SD effects and ABC at the interfaces (air–WM slab and WM slab–ground plane) in the homogenization model for the WM slab with long vias and, mostly im-

Authorized licensed use limited to: Instituto de Telecomunicacoes. Downloaded on November 15, 2009 at 11:40 from IEEE Xplore. Restrictions apply.

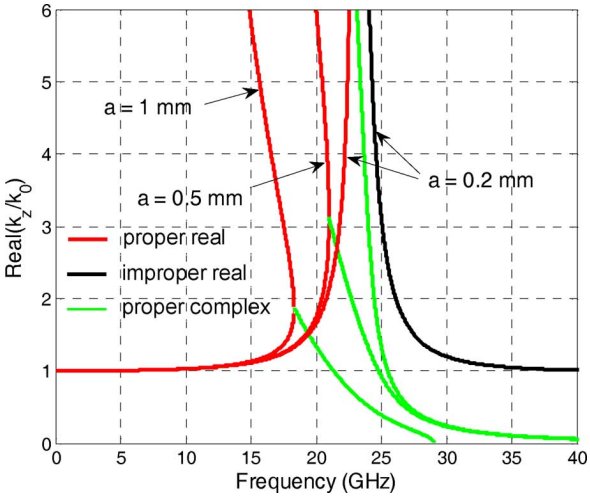

Fig. 12. Dispersion behavior of surface and leaky waves on WM slab with highly dense short vias based on the ENG model. For a small period the ENG model results for a proper real (bound) mode agree with those obtained by the SD+ABC model shown in Fig. 10.

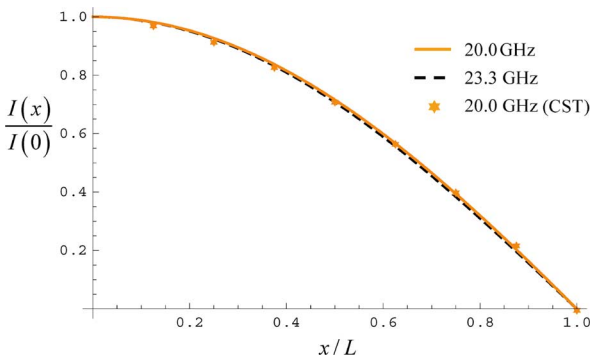

Fig. 13. Normalized magnitude of the microscopic current along the vias calculated for the first proper real TM^z surface-wave mode with the dispersion behavior shown in Fig. 8. The current profile is practically independent of frequency. The discrete star-shaped symbols were calculated using the full-wave simulator CST Microwave Studio [46].

portant, with *short vias*, is critical in order to accurately capture the physics of surface waves and leaky waves. The ENG model is applicable only in the case of highly dense vias structure, where the WM slab acts as a material with extreme anisotropy. The WM slab supports proper complex backward and improper complex forward leaky waves (as predicted by the SD+ABC model). In general, the leaky waves predicted by the ENG model do not describe correctly the dynamics of the leaky waves of the actual WM slab, leading to the conclusion that the WM slab cannot be modeled as an ENG material. Only in the case of WM slab with highly dense vias the leaky-wave behavior predicted by both the ENG and SD+ABC models agrees (however, in this case, the leaky mode is nonphysical due to a large attenuation constant). It should be noted that a true ENG slab (in air) in general can support physical backward and complex modes [47].

B. Surface Waves and Leaky Waves on Mushroom Structures

1) Mushroom Structures With Long Vias: In the first example, the mushroom structure with long vias connected to the patch array (with the geometry shown in Fig. 2) is studied for

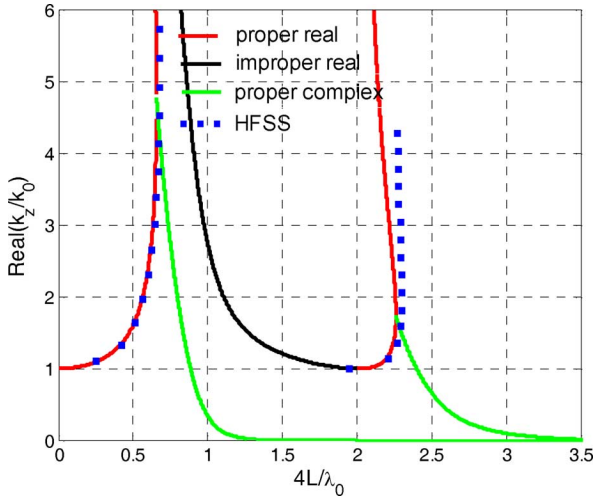

Fig. 14. Dispersion behavior of TM^z surface-wave and leaky-wave modes on mushroom structure with long vias based on the SD+ABC model. The modal spectrum consists of proper real (bound), improper real, and proper complex leaky-wave modes.

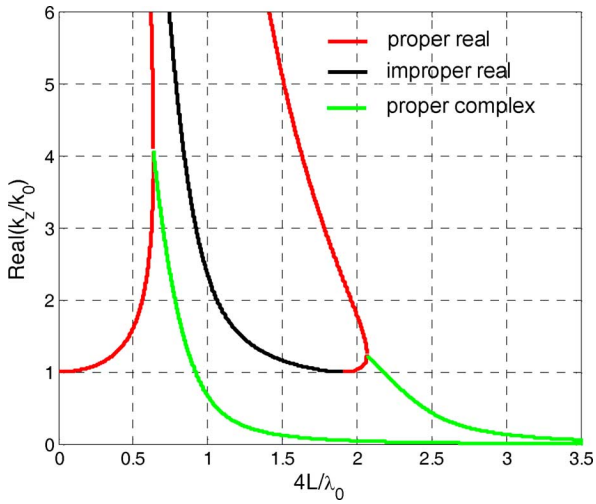

Fig. 15. Dispersion behavior of TM^z surface-wave and leaky-wave modes on mushroom structure with long vias based on the ENG approximation model.

the following parameters: $a = 1$ mm, $L = 5$ mm, $g = 0.1$ mm, $r_0 = 0.05$ mm, and $\varepsilon_r = 1$. The dispersion behavior of TM^z surface-wave and leaky-wave modes obtained by the SD+ABC homogenization model is shown in Fig. 14, and compared with the HFSS results (a good agreement is observed, especially for the first TM^z surface-wave mode). The modal spectrum consists of proper real (forward and backward), improper real, and proper complex (leaky) backward modes. The imaginary part of the complex modes is omitted here. The dispersion behavior of the real and complex solutions will be explained in detail in the example of a mushroom structure with short vias.

The results of surface-wave and leaky-wave behavior obtained with the ENG approximation model are shown in Fig. 15. It can be seen that, at very low frequencies, there is a good agreement of the proper real and proper complex solutions obtained with the two models (Figs. 14 and 15); however, with the increase of frequency, the dispersion behavior becomes different. It should be noted that, for this example with long

Authorized licensed use limited to: Instituto de Telecomunicacoes. Downloaded on November 15, 2009 at 11:40 from IEEE Xplore. Restrictions apply.

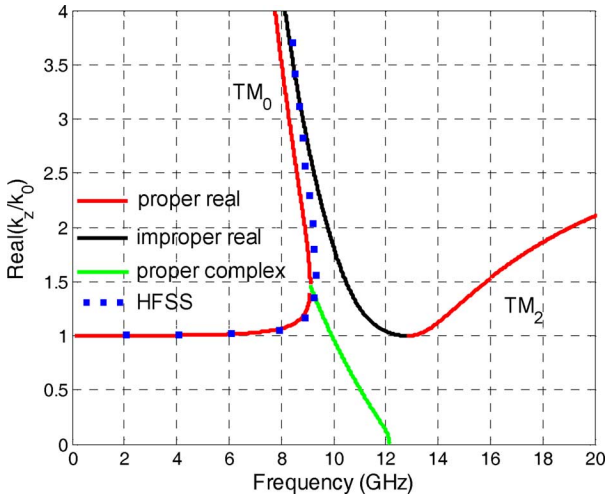

Fig. 16. Dispersion behavior of the TM^z surface-wave and leaky-wave modes on mushroom structure with short vias based on the SD+ABC model. At the frequency corresponding to the left bound of the stopband for proper real modes, backward radiation occurs associated with the leaky-wave cutoff of the proper complex mode. HFSS results are also shown for comparison for the first proper forward and proper backward real modes, indicating a good agreement with the homogenization results.

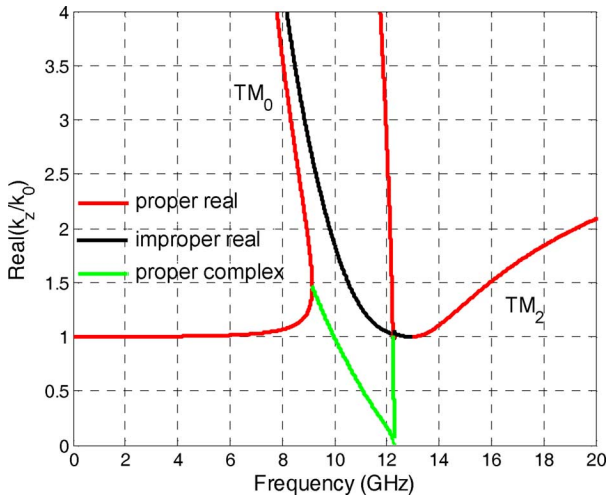

Fig. 17. Dispersion behavior of the TM^z surface-wave and leaky-wave modes on mushroom structure with short vias based on the ENG approximation model. A very good agreement is observed with the SD+ABC results shown in Fig. 16, except for a narrow frequency range close to the plasma frequency around 12 GHz, where the ENG approximation fails.

vias, the inclusion of SD in the SD+ABC homogenization model is critical, and the ENG approximation model (which does not consider the SD effects) fails as we approach the plasma frequency of 92.13 GHz. In fact, for this example, the current along the vias is nonuniform, and thus, in light of previous considerations, the SD effects may be suppressed only when the material is characterized by extreme anisotropy (i.e., for low frequencies).

2) Mushroom Structures With Short Vias: In the next example, we consider a mushroom structure on a high-index dielectric substrate with short vias (Fig. 2), characterized by the following parameters: $a = 2$ mm, $L = 1$ mm, $g = 0.2$ mm, $r_0 = 0.05$ mm, and $\varepsilon_r = 10.2$. The dispersion behavior of the TM^z surface-wave and leaky-wave modes obtained with the SD+ABC homogenization model, including proper real and proper complex solutions, is shown in Fig. 16. The natural TM^z modes of the periodic mushroom HIS structure are defined here as TM_0 and TM_2 to be consistent with the terminology used in the dielectric slab waveguide (as the corresponding unperturbed structure). At low frequencies, the TM_0 proper real (bound) mode propagates primarily in the air region and weakly interacts with the mushroom structure ($\mathrm{Re}\{k_z/k_0\}$ is close to 1). The mode propagates in the forward $+z$-direction (both phase and group velocities are along the same $+z$-direction: $d(\mathrm{Re}\{k_z\})/df > 0$). There is also another proper real TM_0 mode, which is highly dispersive and strongly interacts with the mushroom structure (the field is primarily concentrated below the patches). This mode propagates in the backward $-z$-direction (the phase velocity is positive and the group velocity is negative: $d(\mathrm{Re}\{k_z\})/df < 0$). At the frequency of 9.11 GHz, the phase velocities of the forward and backward modes become equal (the vertical slope of dispersion curves is the same) and the propagation of proper real (bound) modes stops, which corresponds to the left bound of the stopband for the proper real TM^z modes. In Fig. 16, the proper real forward TM_2 mode is also shown, and the cutoff frequency of that mode at approximately 12.78 GHz corresponds to the right bound of the stopband for the proper real TM^z modes. As was mentioned before, the analysis in this paper is limited to the TM^z natural modes only since the TE^z modes do not interact with vias and propagate as in the HIS structure without vias (with the results presented in [23]–[25]). Of course, with the TE^z waves considered, we can also define a stopband for proper real TM^z and TE^z waves.

At the frequency of 9.11 GHz (where the propagation for bound modes stops), backward radiation occurs associated with the cutoff frequency of the proper complex leaky mode (defined on the proper Riemann sheet in the complex k_z-plane with the field decaying in the x-direction as $e^{-\gamma_0 x}$, $\mathrm{Re}\{\gamma_0\} > 0$) [22], [48]. It should be noted that backward radiation appears within the stopband of proper real TM^z modes (Fig. 16); however, it can continue outside of the stopband for TM^z and TE^z modes (not shown here). The physical radiation also occurs when the proper complex mode enters a fast-wave regime when $\mathrm{Re}\{k_z/k_0\} < 1$ and the imaginary part of the propagation constant (as attenuation constant) is small in comparison to the values of the real part (the results for the imaginary part will be shown later in this section).

This example of the mushroom structure with short vias has been also studied using the local homogenization model (ENG approximation), and the results for TM^z surface-wave and leaky-wave propagation are shown in Fig. 17. An important observation is that the results of the two homogenization models (proper and improper, real and complex solutions) shown in Figs. 16 and 17 agree very well in a wide frequency range, except for a very narrow band in the vicinity of the plasma frequency around 12 GHz, where the ENG approximation fails (due to the singularity in (8) where $\varepsilon_{xx} = 0$). This is reflected in Fig. 17 as fictitious higher order modes (proper real and proper complex). In practice, these spurious solutions may be significantly damped by introducing a small loss in the permittivity of the host material ε_r.

Authorized licensed use limited to: Instituto de Telecomunicacoes. Downloaded on November 15, 2009 at 11:40 from IEEE Xplore. Restrictions apply.

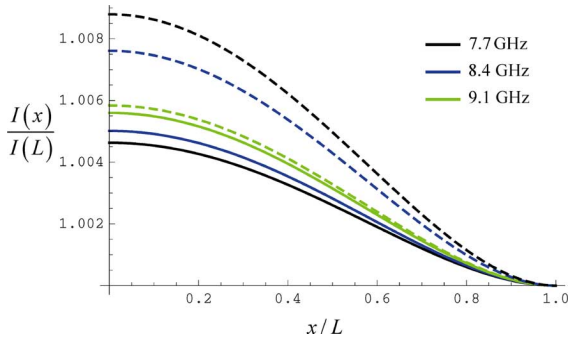

Fig. 18. Normalized magnitude of the microscopic current along the vias calculated for the proper real forward (solid lines) and proper real backward (dashed lines) TM_0 surface-wave modes with the dispersion behavior shown in Fig. 16. The current is practically uniform.

In order to have a better understanding of such agreement in the results given by the nonlocal and local homogenization models, the behavior of the current along the vias has been studied. The microscopic current along a generic via is calculated in terms of the averaged (macroscopic) electric and magnetic fields of the mushroom structure based on the SD+ABC model as (21), and the results for the current normalized magnitude are shown in Fig. 18. The current is calculated at several frequencies for proper forward and proper backward TM_0 surface wave modes with the dispersion behavior shown in Fig. 16. It can be seen that the current is very much uniform for both proper real modes at different frequencies (even at the frequency of 9.1 GHz very close to the left bound of the first stopband of TM^z modes), showing a distinctively different behavior as compared to the WM slab (Fig. 13). This observation in the current behavior leads to the conclusion that, in the mushroom HIS structures with short vias, the SD effects may be significantly reduced by connecting the metallic patches to the vias. The physics of reduction of SD can be explained as follows. When the metallic patches are considerably larger than the diameter of the metallic vias, the electric charges will no longer accumulate on the tips of the vias, but spread over the metallic patches. Therefore, in electrically thin WM substrates with vias connected to the ground and the metallic patches, the charge density along the vias is approximately zero, resulting in nearly uniform currents along the vias. This is because the electromagnetic fields are nearly uniform along the direction of the wires, and thus the spectral amplitude of the fields (in the Fourier domain) has a peak at $k_x \approx 0$, for which the nonlocal dielectric function is coincident with the ENG model. Of course, this applies only to short vias, and in the case of long vias, the results by the SD+ABC model and the ENG approximation shown in Figs. 14 and 15 are different (especially at higher frequencies). In the case of short vias with uniform current, the ENG model of the WM slab (and consequently the mushroom-type HIS structures) is adequate to model the physics of surface-wave propagation, and the WM slab can be regarded as an uniaxial ENG material.

An important observation concerns the transition from the backward to forward radiation associated with proper complex and improper complex leaky-wave modes. In Fig. 16, it can be seen that the propagation constant of the proper complex mode

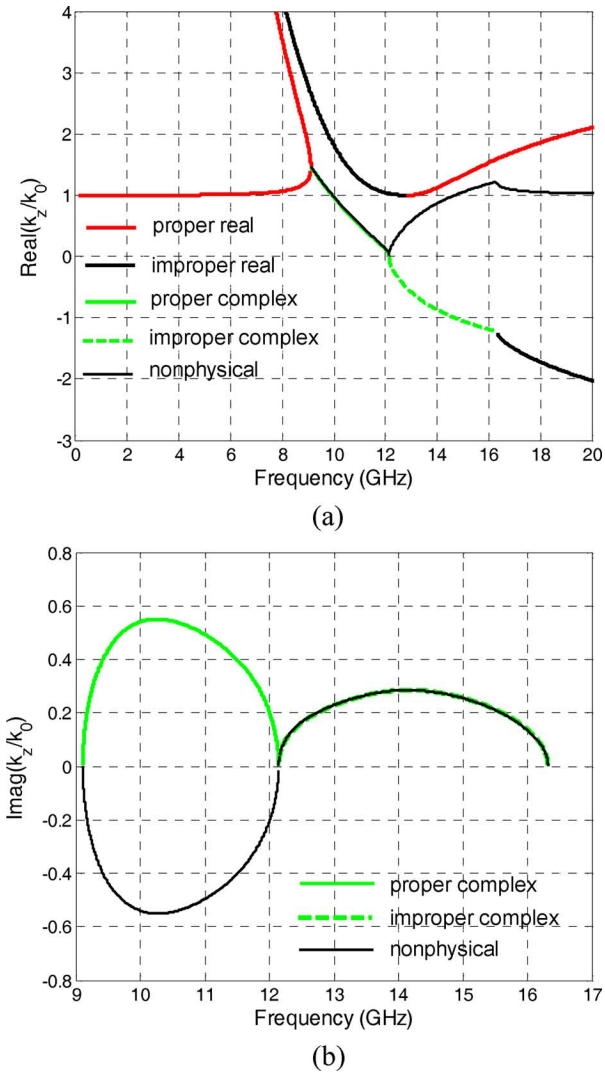

Fig. 19. Dispersion behavior of TM^z surface-wave and leaky-wave modes in the mushroom structure with short vias, showing a transition from the proper complex to improper complex leaky-wave modes associated with backward and forward radiation, respectively. (a) Real part of the normalized propagation constant. (b) Imaginary part of the normalized propagation constant.

approaches zero at the plasma frequency of 12.14 GHz. In fact, this is consistent with the modal classification in metamaterial slabs [49] such that an ENG slab (a double-negative slab as well) supports TM proper complex modes, whereas μ-negative and double-positive slabs support TM improper complex modes.

By increasing frequency above the plasma frequency, the proper complex mode becomes an improper complex mode, as is shown in Fig. 19. In general, we have poles of the complex modes defined in four quadrants of the complex propagation constant plane, and the results of the dispersion behavior in Fig. 19 are related to the pole dynamics in the complex k_z-plane (it should be noted that only two poles, which originate in the spectral gap region with $\mathrm{Re}\{k_z/k_0\} > 0$ at 9.11 GHz, are considered here). The proper complex leaky backward mode as a physical solution (exponentially decaying along the propagation direction) is defined in the first quadrant of the complex k_z-plane such that $\mathrm{Re}\{k_z/k_0\}\mathrm{Im}\{k_z/k_0\} > 0$ [22], [48], and it propagates in the $-z$-direction (with positive phase velocity

Authorized licensed use limited to: Instituto de Telecomunicacoes. Downloaded on November 15, 2009 at 11:40 from IEEE Xplore. Restrictions apply.

due to $\mathrm{Re}\{k_z/k_0\} > 0$ and negative group velocity due to the negative slope of the dispersion curve). There is also a nonphysical proper complex mode (exponentially growing along the propagation direction), which is defined in the fourth quadrant of the complex k_z-plane, as a complex conjugate of the physical solution such that $\mathrm{Re}\{k_z/k_0\}\mathrm{Im}\{k_z/k_0\} < 0$. A more general definition of physical and nonphysical solutions is determined by an excitation problem where the radiated field is obtained either by spectral or nonspectral representations [49] such that the physical leaky-wave poles contribute to the radiated field (calculated as an integral along the steepest descent path).

As the physical proper complex mode shown in Fig. 19 enters its fast-wave regime ($0 < \mathrm{Re}\{k_z/k_0\} < 1$), it radiates in free space in the $+z$-direction in the sense of a leaky-wave backward radiation in the frequency range where $\mathrm{Im}\{k_z/k_0\}$ is relatively small in comparison with $\mathrm{Re}\{k_z/k_0\}$ (for large values of $\mathrm{Im}\{k_z/k_0\}$, the wave attenuates and does not radiate). At the plasma frequency, both $\mathrm{Re}\{k_z/k_0\}$ and $\mathrm{Im}\{k_z/k_0\}$ are equal to zero (with the vertical slope of the dispersion curve), which corresponds to the open-stopband null point of the proper complex solutions (physical and nonphysical). At the open-stopband point, the attenuation constant of the leaky mode drops to zero, as it can be also observed in 1-D printed leaky-wave antennas [50] and 2-D printed periodic structures [22], which results in the absense of radiation. However, an excitation problem should be solved to understand the radiation mechanism in this case.

As the frequency is increased above the plasma frequency, the proper complex poles cross the Sommerfeld branch cut so that the physical pole from the first quadrant migrates to the second quadrant as the improper complex leaky forward physical mode (defined on the improper Riemann sheet), and the nonphysical pole from the fourth quadrant migrates to the first quadrant as the nonphysical improper complex mode (also defined on the improper Riemann sheet). As the physical improper complex mode enters the fast wave regime ($-1 < \mathrm{Re}\{k_z/k_0\} < 0$), it radiates in free space in the $-z$-direction (in contrast to a proper complex mode, which radiates in the $+z$-direction), but is understood in the sense of a forward leaky wave because both the phase and group velocities are negative (as can be seen in Fig. 19). At the frequency of 16.23 GHz, the physical and nonphysical improper complex modes are below cutoff turning to improper real solutions.

Regarding the nonphysical solutions, it should be noted that the slope of the dispersion curves changes from backward to forward in contrast to the same negative slope in the physical proper complex and improper complex solutions [see Fig. 19(a)]. Also, in order to understand which branch to follow (physical or nonphysical) at leaky-wave cutoff frequencies, small losses were introduced in the permittivity of the host material. It is observed that starting at low frequencies, a proper real forward mode follows a nonphysical branch and the proper real backward mode turns to the physical proper complex mode. However, at higher frequencies above 20 GHz (not shown here), a nonphysical improper mode eventually will turn to a physical proper real higher order forward mode (after passing the cutoff frequency at $\mathrm{Re}\{k_z/k_0\} = 1$ by crossing the Sommerfeld branch cut). This means that there is a very large "spectral gap" frequency region [48] between two physical proper real forward modes, connected by a nonphysical solution.

The current behavior has also been studied for proper complex and improper complex modes (not shown here). It is observed that for both complex modes, the current is nearly uniform over the frequency regimes of these modes (Fig. 19), and at the plasma frequency, the normalized magnitude along the vias is equal to 1.

V. Conclusions

A nonlocal (SD+ABC) homogenization model has been proposed for the characterization of the spectrum of natural TM^z surface-wave and leaky-wave modes on mushroom-type HIS structures. The mushroom structures are modeled as a WM slab attached to a metallic grid (a patch array). In this regard, the analysis of surface-wave and leaky-wave propagation on WM slabs (with no metallic grid) by the local (ENG approximation) and nonlocal (SD+ABC) homogenization models is essential for the understanding of modal properties of mushroom structures. It is shown that the inclusion of SD effects in the homogenization model of the WM slab is critical in order to accurately capture the physics of surface-wave and leaky-wave propagation, whereas the ENG approximation fails not only for the WM slab with long vias, but also with short vias, except in the regime where the WM behaves as a material with extreme anisotropy (i.e., for very low frequencies or when the wires are very densely packed). It is shown that WM slabs may support proper complex backward and improper complex forward leaky waves, and that the ENG approximation does not predict correctly the behavior of leaky waves. Only in the case of a WM slab with highly dense vias the ENG model gives correct results for leaky waves (which agree with the SD+ABC model; however, these modes are nonphysical due to large attenuation constant). Based on the understanding of surface-wave and leaky-wave behavior on WM slabs, surface-wave and leaky-wave characteristics have been studied in mushroom-type HIS structures with long and short vias. An interesting observation is that, in the case of mushroom structures with short vias, the results of the SD+ABC model and the ENG approximation agree very well for surface-wave and leaky-wave modes, except for a narrow frequency range close to the plasma frequency, where the ENG approximation fails. The agreement in the results of nonlocal and local homogenization models is due to the significant reduction of SD effects in the WM slab, justified by the presence of metallic grid attached to the vias, resulting in the nearly uniform current along the vias.

There are also several important observations regarding the modal spectrum of mushroom structures. In particular, it is shown that the modal spectrum includes proper real forward and backward modes and proper complex and improper complex modes. A stopband of proper real modes at low frequencies is due to occurrence of a TM^z backward proper complex leaky wave associated with the WM slab and capacitive grid. The transition of proper complex modes to improper complex modes occurs at the plasma frequency, associated with backward and forward leaky-wave radiation.

Authorized licensed use limited to: Instituto de Telecomunicacoes. Downloaded on November 15, 2009 at 11:40 from IEEE Xplore. Restrictions apply.

ACKNOWLEDGMENT

Author A. Yakovlev would like to acknowledge helpful discussions with P. Baccarelli, "La Sapienza" University of Rome, Rome, Italy, G. W. Hanson, University of Wisconsin–Milwaukee, S. Hrabar, University of Zagreb, Zagreb, Croatia, concerning the backward and forward radiation on mushroom HIS structures. The authors also thank the reviewers for several valuable and insightful comments.

REFERENCES

[1] B. A. Munk, *Frequency Selective Surfaces: Theory and Design*. New York: Wiley, 2000.

[2] D. Sievenpiper, L. Zhang, R. F. J. Broas, N. G. Alexopolous, and E. Yablonovitch, "High-impedance electromagnetic surfaces with a forbidden frequency band," *IEEE Trans. Microw. Theory Tech.*, vol. 47, no. 11, pp. 2059–2074, Nov. 1999.

[3] D. Sievenpiper, "High-impedance electromagnetic surfaces," Ph.D. dissertation, Dept. Elect. Eng., Univ. California at Los Angeles, Los Angeles, CA, 1999.

[4] S. A. Tretyakov and C. R. Simovski, "Dynamic model of artificial reactive impedance surfaces," *J. Electromagn. Waves Appl.*, vol. 17, no. 1, pp. 131–145, 2003.

[5] Y. Zhang, J. von Hagen, M. Younis, C. Fischer, and W. Weisbeck, "Planar artificial magnetic conductors and patch antennas," *IEEE Trans. Antennas Propag.*, vol. 51, no. 10, pp. 2704–2712, Oct. 2003.

[6] G. Goussetis, A. P. Feresidis, and J. C. Vardaxoglou, "Tailoring the AMC and EBG characteristics of periodic metallic arrays printed on grounded dielectric substrate," *IEEE Trans. Antennas Propag.*, vol. 54, no. 1, pp. 82–89, Jan. 2006.

[7] O. Luukkonen, C. Simovski, G. Granet, G. Goussetis, D. Lioubtchenko, A. V. Raisanen, and S. A. Tretyakov, "Simple and accurate analytical model of planar grids and high-impedance surfaces comprising metal strips or patches," *IEEE Trans. Antennas Propag.*, vol. 56, no. 6, pp. 1624–1632, Jun. 2008.

[8] S. Maci and P.-S. Kildal, "Hard and soft Gangbuster surfaces," in *Proc. URSI Int. Electromagn. Theory Symp.*, Pisa, Italy, May 2004, pp. 290–292.

[9] S. Maci, M. Caiazzo, A. Cucini, and M. Casaletti, "A pole-zero matching method for EBG surfaces composed of a dipole FSS printed on a grounded dielectric slab," *IEEE Trans. Antennas Propag.*, vol. 53, no. 1, pp. 70–81, Jan. 2005.

[10] G. Goussetis, Y. Guo, A. P. Feresidis, and J. C. Vardaxoglou, "Miniaturized and multi-band artificial magnetic conductors and electromagnetic band gap surfaces," in *Proc. IEEE AP-S Int. Symp.*, Jun. 2004, vol. 1, pp. 293–296.

[11] M. Hiranandani, A. B. Yakovlev, and A. A. Kishk, "Artificial magnetic conductors realized by frequency selective surfaces on a grounded dielectric slab for antenna applications," *Proc. Inst. Elect. Eng.—Microw. Antennas Propag.*, vol. 153, no. 5, pt. H, pp. 487–493, 2006.

[12] D. J. Kern, D. H. Werner, A. Monorchio, L. Lanuzza, and M. J. Wilhelm, "The design synthesis of multiband artificial magnetic conductors using high impedance frequency selective surfaces," *IEEE Trans. Antennas Propag.*, vol. 53, no. 1, pp. 8–17, Jan. 2005.

[13] F. Yang and Y. Rahmat-Samii, "Reflection phase characterization of the EBG ground plane for low profile wire antenna applications," *IEEE Trans. Antennas Propag.*, vol. 51, no. 10, pp. 2691–2703, Oct. 2003.

[14] A. P. Feresidis, G. Goussetis, S. Wang, and J. C. Vardaxoglou, "Artificial magnetic conductor surfaces and their application to low-profile high-gain planar antennas," *IEEE Trans. Antennas Propag.*, vol. 53, no. 1, pp. 209–215, Jan. 2005.

[15] F.-R. Yang, K.-P. Ma, Y. Qian, and T. Itoh, "A novel TEM waveguide using uniplanar compact photonic-bandgap (UC-PBG) structure," *IEEE Trans. Microw. Theory Tech.*, vol. 47, no. 11, pp. 2092–2098, Nov. 1999.

[16] V. A. Klymko, A. B. Yakovlev, I. A. Eshrah, A. A. Kishk, and A. W. Glisson, "Dyadic Green's function of an ideal hard surface circular waveguide with application to excitation and scattering problems," *Radio Sci.*, vol. 40, no. 3, Jun. 2005, RS3014, 10.1029/2004RS003167.

[17] W. Huang, A. B. Yakovlev, A. A. Kishk, A. W. Glisson, and I. A. Eshrah, "Green's function analysis of an ideal hard surface rectangular waveguide," *Radio Sci.*, vol. 40, Sep. 2005, RS5006, 10.1029/2004RS003161.

[18] S. A. Tretyakov and S. I. Maslovski, "Thin absorbing structure for all incident angles based on the use of a high-impedance surface," *Microw. Opt. Technol. Lett.*, vol. 38, no. 3, pp. 175–178, 2003.

[19] Q. Gao, Y. Yin, D.-B. Yan, and N.-C. Yuan, "A novel radar-absorbing-material based on EBG structure," *Microw. Opt. Technol. Lett.*, vol. 47, no. 3, pp. 228–230, 2005.

[20] D. F. Sievenpiper, J. H. Schaffner, H. J. Song, R. Y. Loo, and G. Tangonan, "Two-dimensional beam steering using an electrically tunable impedance surface," *IEEE Trans. Antennas Propag.*, vol. 53, no. 10, pp. 2713–2722, Oct. 2003.

[21] O. Luukkonen, C. R. Simovski, A. V. Räisänen, and S. A. Tretyakov, "An efficient and simple analytical model for analysis of propagation properties in impedance waveguides," *IEEE Trans. Microw. Theory Tech.*, vol. 56, no. 7, pp. 1624–1632, Jul. 2008.

[22] P. Baccarelli, S. Paulotto, and C. Di Nallo, "Full-wave analysis of bound and leaky modes propagating along 2D periodic printed structures with arbitrary metallisation in the unit cell," *IET Microw. Antennas Propag.*, vol. 1, no. 1, pp. 217–225, 2007.

[23] A. B. Yakovlev, C. R. Simovski, S. A. Tretyakov, O. Luukkonen, G. W. Hanson, S. Paulotto, and P. Baccarelli, "Analytical modeling of surface waves on high impedance surfaces," in *Proc. NATO Adv. Res. Workshop: Metamater. Secure Inform. Commun. Technol.*, Marrakesh, Morocco, May 2008, pp. 184–193.

[24] O. Luukkonen, A. B. Yakovlev, C. R. Simovski, and S. A. Tretyakov, "Comparative study of surface waves on high-impedance surfaces with and without vias," in *Proc. IEEE AP-S Int. Symp.*, Jul. 2008, pp. 1–4.

[25] A. B. Yakovlev, O. Luukkonen, C. R. Simovski, S. A. Tretyakov, S. Paulotto, P. Baccarelli, and G. W. Hanson, "Analytical modeling of surface waves on high impedance surfaces," in *Metamaterials and Plasmonics: Fundamentals, Modeling, Applications*, S. Zouhdi, A. Sihvola, and A. P. Vinogradov, Eds. Berlin, Germany: Springer, 2009, pp. 239–254.

[26] S. A. Tretyakov, *Analytical Modeling in Applied Electromagnetics*. Boston, MA: Artech House, 2003.

[27] A. Grbic and G. V. Eleftheriades, "Dispersion analysis of a microstrip-based negative refractive index periodic structure," *Microw. Wireless Compon. Lett.*, vol. 13, no. 4, pp. 155–157, Apr. 2003.

[28] S. Clavijo, R. E. Díaz, and W. E. McKinzie, "Design methodology for Sievenpiper high-impedance surfaces: An artificial magnetic conductor for positive gain electrically small antennas," *IEEE Trans. Antennas Propag.*, vol. 51, no. 10, pp. 2678–2690, Oct. 2003.

[29] M. G. Silveirinha, C. A. Fernandes, and J. R. Costa, "Electromagnetic characterization of textured surfaces formed by metallic pins," *IEEE Trans. Antennas Propag.*, vol. 56, no. 2, pp. 405–415, Feb. 2008.

[30] C. R. Simovski, P. de Maagt, and I. V. Melchakova, "High-impedance surfaces having stable resonance with respect to polarization and incidence angle," *IEEE Trans. Antennas Propag.*, vol. 53, no. 3, pp. 908–914, Mar. 2005.

[31] G. Shvets, "Photonic approach to making a surface wave accelerator," in *Proc. 10th Adv. Accelerator Concepts Workshop*, 2002, vol. 647, pp. 371–382.

[32] P. A. Belov, R. Marques, S. I. Maslovski, I. S. Nefedov, M. G. Silveirinha, C. R. Simovski, and S. A. Tretyakov, "Strong spatial dispersion in wire media in the very large wavelength limit," *Phys. Rev. B, Condens. Matter*, vol. 67, 2003, Art. ID 113103.

[33] M. G. Silveirinha and C. A. Fernandes, "Homogenization of 3-D-connected and nonconnected wire metamaterials," *IEEE Trans. Microw. Theory Tech.*, vol. 53, no. 4, pp. 1418–1430, Apr. 2005.

[34] M. G. Silveirinha, "Additional boundary condition for the wire medium," *IEEE Trans. Antennas Propag.*, vol. 54, no. 6, pp. 1766–1780, Jun. 2006.

[35] M. G. Silveirinha, C. A. Fernandes, and J. R. Costa, "Additional boundary condition for a wire medium connected to a metallic surface," *New J. Phys.*, vol. 10, no. 053011, pp. 1–17, 2008.

[36] I. S. Nefedov and A. J. Viitanen, "Guided waves in uniaxial wire medium slab," in *PIER*, 2003, vol. 51, pp. 167–185.

[37] I. S. Nefedov, A. J. Viitanen, and S. A. Tretyakov, "Propagating and evanescent modes in 2-D wire media," *Phys. Rev. E, Stat. Phys. Plasmas Fluids Relat. Interdiscip. Top.*, vol. 71, pp. 046612-1–046612-10, 2005.

[38] I. S. Nefedov, X. Darbenne, C. Craeye, and S. A. Tretyakov, "Backward waves in a waveguide, filled with wire media," *Microw. Opt. Technol. Lett.*, vol. 48, pp. 2560–2564, 2006.

[39] P. Burghignoli, G. Lovat, F. Capolino, D. R. Jackson, and D. R. Wilton, "Modal propagation and excitation on a wire-medium slab," *IEEE Trans. Microw. Theory Tech.*, vol. 56, no. 5, pp. 1112–1124, May 2008.

Authorized licensed use limited to: Instituto de Telecomunicacoes. Downloaded on November 15, 2009 at 11:40 from IEEE Xplore. Restrictions apply.

[40] P. Burghignoli, G. Lovat, F. Capolino, D. R. Jackson, and D. R. Wilton, "Directive leaky-wave radiation from a dipole source in a wire-medium slab," *IEEE Trans. Antennas Propag.*, vol. 56, no. 5, pp. 1329–1339, May 2008.
[41] A. Demetriadou and J. B. Pendry, "Taming spatial dispersion in wire metamaterial," *J. Phys., Condens. Matter*, vol. 20, 2008, Art. ID 295222.
[42] A. B. Yakovlev, M. G. Silveirinha, O. Luukkonen, C. R. Simovski, I. S. Nefedov, and S. A. Tretyakov, "Homogenization models for the analysis of surface waves on mushroom structures," in *Proc. 2nd Int. Adv. Electromagn. Mater. Microw. Opt. Congr.*, Pamplona, Spain, Sep. 2008, pp. 310–312.
[43] O. Luukkonen, M. G. Silveirinha, A. B. Yakovlev, C. R. Simovski, I. S. Nefedov, and S. A. Tretyakov, "Homogenization models for the analysis of reflection properties of mushroom structures," in *Proc. 2nd Int. Adv. Electromagn. Mater. Microw. Opt. Congr.*, Pamplona, Spain, Sep. 2008, pp. 208–210.
[44] C. R. Simovski, S. Zouhdi, and V. V. Yatsenko, "Electromagnetic interaction in dipole grids and prospective high-impedance surfaces," *Radio Sci.*, vol. 40, 2005, RS5008, 10.1029/2004RS003064.
[45] High Frequency Structure Simulator (HFSS) ver. 9.2.1, Ansoft Corporation, Pittsburgh, PA, 2004. [Online]. Available: http://ansoft.com
[46] CST Microwave Studio CST GmbH, Darmstadt, Germany, 2008. [Online]. Available: http://www.cst.com
[47] A. Alù and N. Engheta, "Optical nanotransmission lines: Synthesis of planar left-handed metamaterials in the infrared and visible regimes," *J. Opt. Soc. Amer. B, Opt. Phys.*, vol. 23, no. 3, pp. 571–583, 2006.
[48] T. Tamir and A. A. Oliner, "Guided complex waves. Part I: Fields at an interface," *Proc. Inst. Elect. Eng.*, vol. 110, pp. 310–334, 1963.
[49] P. Baccarelli, P. Burghignoli, F. Frezza, A. Galli, P. Lampariello, G. Lovat, and S. Paulotto, "Effects of leaky-wave propagation in metamaterial grounded slabs excited by a dipole source," *IEEE Trans. Microw. Theory Tech.*, vol. 53, no. 1, pp. 32–44, Jan. 2005.
[50] S. Paulotto, P. Baccarelli, F. Frezza, and D. R. Jackson, "A novel technique to eliminate the open stopband in 1-D periodic printed leaky-wave antennas," in *Proc. EuCAP 2007*, Edinburgh, U.K., Nov. 2007, pp. 1–5.

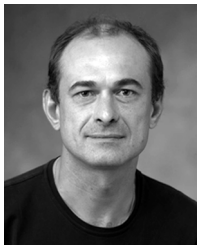

Alexander B. Yakovlev (S'94–M'97–SM'01) received the Ph.D. degree in radiophysics from the Institute of Radiophysics and Electronics, National Academy of Sciences, Kiev, Ukraine, in 1992, and the Ph.D. degree in electrical engineering from the University of Wisconsin at Milwaukee, in 1997.

In 2000, he joined the Department of Electrical Engineering, The University of Mississippi, as an Assistant Professor, and became an Associate Professor in 2004. He coauthored *Operator Theory for Electromagnetics: An Introduction* (Springer, 2002). From 2003 to 2006, he was an Associate Editor-in-Chief of the *ACES Journal*. His research interests include mathematical methods in applied electromagnetics, homogenization models for metamaterials, artificial impedance surfaces, and EBG structures, theory of leaky waves, and catastrophe and bifurcation theories.

Dr. Yakovlev is a member of URSI Commission B. From 2005 to 2008, he was an associate editor of the IEEE TRANSACTIONS ON MICROWAVE THEORY AND TECHNIQUES. He was the recipient of the Young Scientist Award presented at the 1992 URSI International Symposium on Electromagnetic Theory, Sydney, Australia, and the Young Scientist Award presented at the 1996 International Symposium on Antennas and Propagation, Chiba, Japan.

Mário G. Silveirinha (S'99–M'03) received the Licenciado degree in electrical engineering from the Universidade de Coimbra, Coimbra, Portugal, in 1998, and the Ph.D. degree in electrical and computer engineering from the Instituto Superior Técnico (IST), Technical University of Lisbon, Lisbon, Portugal, in 2003.

Since 2003, he has been an Assistant Professor with the Universidade de Coimbra. His research interests include electromagnetic wave propagation in structured materials and homogenization theory.

Olli Luukkonen received the M.Sc. degree in electrical engineering from the TKK Helsinki University of Technology, Espoo, Finland, in 2006, and is currently working toward the Ph.D. degree at the TKK Helsinki University of Technology.

He is currently a Research Engineer with the Department of Radio Science and Engineering, TKK Helsinki University of Technology. His current research interests include artificial electromagnetic materials, surfaces, and their applications.

Constantin R. Simovski (M'92) was born in Leningrad, Russian Republic of Soviet Union (now St. Petersburg), Russia, on December 7, 1957. He received the Diploma of Engineer Researcher degree in radio engineering, the Ph.D. degree in electromagnetic theory, and Doctor of Sciences degree from the St. Petersburg State Polytechnic University (formerly the Leningrad Polytechnic Institute and State Technical University), St. Petersburg, Russia, in 1980, 1986, and 2000, respectively. In 1986, he defended the thesis of a Candidate of Science (Ph.D.) (a study of the scattering of Earth waves in the mountains) at the Leningrad Polytechnic Institute. In 2000, he defended the thesis of Doctor of Sciences (a theory of 2-D and 3-D bianisotropic scattering arrays).

From 1980 to 1992, he was with the Soviet scientific and industrial firm Impulse. In 1992, he joined the St. Petersburg University of Information Technologies, Mechanics and Optics, as an Assistant, where from 1994 to 1995, he was an Assistant Professor, from 1995 to 2001, he was an Associate Professor, and since 2001, he has been a Full Professor. Since 1999, he has been involved in the theory and applications of 2-D and 3-D EBG structures for microwave and ultrashort-wave antennas. He is currently with the TKK Helsinki University of Technology, Espoo, Finland, where his research concerns the field of metamaterials for microwave and optical applications including optics of metal nanoparticles.

Igor S. Nefedov (M'92) received the Dipl. Physicist, Candidate of Sciences (Ph.D.), and Doctor of Sciences degrees in radio-physics from Saratov State University (SSU), Saratov, Russia, in 1972, 1981, and 1998, respectively.

From 1975 to 1992, he was with the Research Institute of Mechanics and Physics, SSU. Since 1992, he has been with the Institute of Radio Engineering and Electronics, Russian Academy of Science, Saratov, Russia. He has been a Visiting Professor with the Radio Laboratory, TKK Helsinki University of Technology (2001–2002) and Full Professor with SSU (2003–2004). He has been a Visiting Researcher in Italy, Germany, Poland, France and Belgium. Since 2004, he has been a Senior Researcher with the TKK Helsinki University of Technology. His main scientific interests are electromagnetic field theory, electromagnetics of complex media, and optics.

Sergei A. Tretyakov (M'92–SM'98–F'08) received the Dipl. Engineer-Physicist, Candidate of Sciences (Ph.D.), and Doctor of Sciences degrees in radiophysics from the St. Petersburg State Technical University, St. Petersburg, Russia, in 1980, 1987, and 1995, respectively.

From 1980 to 2000, he was with the Radiophysics Department, St. Petersburg State Technical University. He is currently a Professor of radio engineering with the Department of Radio Science and Engineering, TKK Helsinki University of Technology, Espoo, Finland, and Coordinator of the European Network of Excellence Metamorphose. His main scientific interests are electromagnetic field theory, complex media electromagnetic, and microwave engineering.

Prof. Tretyakov was chairman of the St. Petersburg IEEE Electron Devies (ED)/Microwave Theory and Techniques (MTT)/Antennas and Propagation (AP) Chapter from 1995 to 1998.

Authorized licensed use limited to: Instituto de Telecomunicacoes. Downloaded on November 15, 2009 at 11:40 from IEEE Xplore. Restrictions apply.